

CHAPTER 1

INTRODUCTION

In recent years, the industrial use of model predictive control (MPC) has increased dramatically and the development of MPC resulted in increased capabilities (Qin and Badgwell, 2003). It is not surprising that recent milling control efforts focus on applying MPC to milling circuits. MPC has a number of desirable characteristics when applied to processes with (Chen *et al.*, 2007a)

- large time delays,
- time varying characteristics,
- nonlinearities, and
- constraints on the manipulated and controlled variables

compared to other control formulations. Better performing control is becoming more essential as surge capacity is reduced in modern plant design (Karageorgos *et al.*, 2006). The constraints handling of MPC makes it suitable in preventing mill under-/overload events and the improved performance has a positive effect on the economies of the grinding circuit (Bouche *et al.*, 2005, Van Drunick and Penny, 2006).

Chen *et al.* (2007a) applied hybrid control in the form of override control (ORC) and MPC. Their aim was to control only the product particle size by manipulating the feed rate of ore to the circuit. ORC is used to prevent overload of the mill and obtain an optimal feed rate setpoint. MPC is employed for handling the constraints and time delay of the process.

Chen *et al.* (2009) applied expert system-based adaptive dynamic matrix control (ADMC) to control a ball mill grinding circuit. The controller is a dynamic matrix controller with extra switching logic. The switching logic is based on an expert system to determine the ore hardness in the grinding circuit and choose the appropriate model for the dynamic matrix controller. The advantage of their formulation is that the switching logic can be made arbitrarily complex, without affecting the control computational burden.



Chen *et al.* (2007b) showed that linear MPC, using a complex four-input-four-output model and complex three-input-three-output model (Chen *et al.*, 2008) and applied to a real industrial plant (unnamed iron ore concentrator plant), provides better long-term stable performance than multi-loop decoupled proportional-integral-derivative (PID) control. Ramasamy *et al.* (2005) did comparative simulation studies between de-tuned multiloop proportional-integral (PI) controllers and unconstrained and constrained MPC on a two-input-two-output linear model of a ball mill grinding circuit. Their findings were that MPC performed well under different operating conditions compared to PI control, which produced oscillations and slow settling times.

Valenzuela *et al.* (1994) compared an early form of MPC called dynamic matrix control (DMC) to PI control and learning automata. The three control methods were simulated on a grinding circuit and the authors concluded that DMC provided the best performance of the three control schemes.

Neesse *et al.* (2004) presents a control strategy for hydrocyclones to increase the operating range of the milling circuit. It increases solids recovery from the hydrocyclone to minimise the recirculating load as well as overgrinding.

Galan *et al.* (2002) presented two H_∞ robust linear controllers for a single-input-single-output (SISO) system. The power draw of the mill was controlled by manipulating the feed rate of ore to the mill. The authors found that the design of the controllers were more systematic than for PI control with guarantees on performance and stability. The methodology can also easily be extended to multi-input-multi-output (MIMO). Craig and MacLeod (1995, 1996) implemented a MIMO robust controller on a three-input-three-output model of a run-of-mine (ROM) grinding circuit based on the μ -methodology. They found that regulation of the mill load and product particle size was satisfactory, but the sump level regulation was inadequate. Their conclusion was that the cost of the extra modelling required to quantify the uncertainties needed to implement a μ -controller was too high compared to inverse Nyquist array (INA) controllers that only needed a nominal model and some online tuning. The μ -controller would probably still require online tuning to provide the best performance.

Neural network-based control of grinding circuits is also investigated by Bhaumik *et al.* (1999), Conradie and Aldrich (2001), Duarte *et al.* (1999a, 2001). Duarte *et al.* (1999a, 2001) used three neural networks in the loop, the first one acting as the estimator for the states, the second one as the controller and the third providing predictions of the state trajectory for predictive control. Conradie and Aldrich (2001) use evolutionary reinforcement learning neural control that uses the symbiotic adaptive neuro-evolution (SANE) algorithm. The controller algorithm learns by applying control moves to the system and gets a reward based on how well the control move contributed to achieving the goal. The controller can therefore potentially apply unwanted control moves in order to learn. It is better to train the controller on simulation models to an acceptable level before applying the controller to a real plant.



Najim *et al.* (1995) presented an adaptive controller for a grinding circuit and implemented it for discrete (SISO) loops to reduce the number of parameters to estimate. The authors found that the controllers performed satisfactorily despite the variable interactions in the system. They concluded that adaptive controllers are easier to design and use than fixed structure multivariable controllers. Xingyan *et al.* (1992) presented an adaptive predictive controller that shows good robustness to delay mismatch in the process and the model, as well as robustness to load disturbances.

(Rajamani and Herbst, 1991*a, b*) developed a simplified nonlinear model for the grinding circuit and compared optimal control to PI control. They found the open-loop optimal controller to provide better performance than PI control.

Supervisory control is a second layer of control that optimises the process by calculating optimal setpoint values for the regulatory control layers. Radhakrishnan (1999) presented model-based supervisory control to optimise an economic objective function on-line. Borell *et al.* (1996) presented supervisory control based on expert systems with IF-THEN statements to optimise mill power that increased milling capacity.

Pomerleau *et al.* (2000) studied four control formulations applied to grinding circuits. The four controllers are decentralised PID, algebraic internal model controllers with an explicit decoupler, full multivariable predictive controllers and distributed adaptive predictive controllers. The authors have drawn the following conclusions:

- *“Fixed structure controllers e.g., PID perform as well as model-based controllers for processes where the delay is relatively small compared to the dominant time constant ($\theta < 5T$) since the models are rarely of order higher than two.*
- *Distributed controllers perform as well as multivariable controllers in regulation if the coupling of the process is taken into account in the design and the proper pairing is used for the dynamics required.*
- *Algebraic multivariable controllers perform as well as optimal multivariable controllers and they have exactly the same limitations e.g., perfect decoupling might be impossible.*
- *Algebraic tuning methods may require more know how than optimal controllers, but are easier to implement on an industrial distributed control system (DCS).*
- *Predictive controller and algebraic controllers perform equally in a stochastic environment if there is no noise model available.*
- *Adaptive controllers perform better than fixed controllers for parametric disturbances or soft nonlinearities. It must be noted though that identification is very difficult in regulation where external disturbances act on the process. They also have the advantage of facilitating the tuning principally for distributed controllers.”* (Pomerleau *et al.*, 2000).



Duarte *et al.* (1999b) compared the performance of five multivariable controllers on a grinding circuit, viz. extended horizon adaptive control, pole-placement adaptive control, model reference adaptive control, direct Nyquist array control and sequential loop closing control. The authors studied the controllers theoretically as well as implemented them on a real plant. Their conclusion was that extended horizon adaptive control provided the best performance, but that multivariable control in general improves grinding performance. Duarte *et al.* (1999b) provides a thorough review of the literature on multivariable control applied to grinding circuits.

Earlier work took unmodelled dynamics, parameter variation and nonlinearities into account by using adaptive control (Duarte *et al.*, 1999b) to improve performance. Robust nonlinear MPC (RNMPC) can ensure stability and sustained performance while satisfying constraints on the inputs and the states of nonlinear uncertain systems. The uncertainties in the nonlinear model can be the result of parameter variations, unmodelled dynamics and external disturbances (Mhaskar and Kennedy, 2008).

1.1 MILL CIRCUIT DESCRIPTION

The theoretical part of this study will assume a ROM milling circuit for gold-bearing ore. The circuit is closed and consists of a semi-autogenous (SAG) mill. A typical mill has dimensions of 5 m in diameter and a length of 9 m (Stanley, 1987).

The circuit is fed gold-bearing ore at about 100 tons/hour and grinds it to give a product with 75% to 80% of the particles smaller than a mesh size of 75 μm . The mill discharges through a grate into a sump. Water is added to the sump to dilute the pulp from the mill. The diluted slurry is then pumped to a hydrocyclone that will separate the product from the out-of-specification material.

The hydrocyclone has an internal diameter of 1 m. The out-of-specification material is discharged from the cyclone underflow back to the mill for further grinding. Feed ore, the underflow of the hydrocyclone and water constitute the mill feed. The product is then sent downstream for further liberation of the gold from the ore.

The variables of the mill (Figure 1.1) that can be controlled are the level of the slurry in the sump (SLEV), the product particle-size (PSE) and the mass of material in the mill (LOAD). The inputs to the mill that can be manipulated are the feed-rate of water to the sump (SFW), the flow-rate of slurry to the cyclone (CFF), the feed-rate of solids to the mill (MFS) and the flow-rate of water to the mill inlet (MIW).

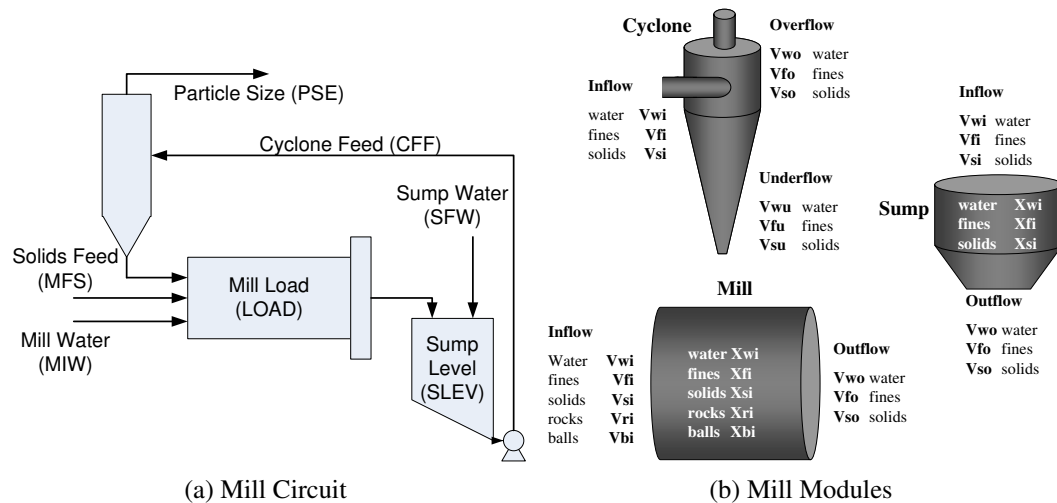


Figure 1.1: ROM closed ore milling circuit.

1.2 OBJECTIVES IN MILL CONTROL

The control of the milling circuit has multiple objectives, firstly to stabilise the system and secondly to optimise the economics of the process (Hulbert, 1989). The economic objective is divided into sub-objectives that each contributes to the overall economic objective of the milling process. A set of possible sub-objectives for the milling circuit is to (Craig and MacLeod, 1995):

- improve product quality
 - by increasing grind fineness, and
 - decreasing the fluctuations in product size,
- maximise throughput,
- minimise the amount of steel that is consumed for each ton of fines produced, and
- minimise the power consumed for each ton of fines produced, etc.

The objectives above are interrelated and require trade-offs to be made. There is a trade-off between the particle size of the product and the throughput of solids (objectives 1a and 2). More gold can be extracted at a finer product size (objective 1a), but the variation in particle size also influences recovery (objective 1b).

It is assumed that the throughput of the mill is maximised when it draws maximum power from the mill motor. The $\Delta LOAD/\Delta MFS$ input-output pair is therefore often under power peak seeking control (Craig *et al.*, 1992b). This is contrary to objective 4, which is to minimise electrical power, but given the value of the milling product versus the cost of electricity, objective 4 is usually considered less important.



Objectives 1 and 3 are interrelated. Steel is added to the mill to stabilise the conditions inside the mill and also to increase throughput. A controller that is capable of stabilising the particle size, will reduce the need for steel and thus objective 3 will be addressed when objective 1b is met.

A possible control strategy is to maximise throughput at a certain particle size setpoint. This strategy considers both objectives 1 and 2. The particle size setpoint may be determined by throughput targets or if throughput is not a consideration, the particle size can be optimised. There is a trade-off between throughput and grind, and grind and residue (product that is not recovered) (Craig *et al.*, 1992b). The main aim of control would usually be to increase throughput while keeping the grind constant.

1.3 AIMS AND OBJECTIVES

The main aim of this thesis is to determine the feasibility of applying robust nonlinear model predictive control to an industrial problem such as the run-of-mine ore milling circuit. To this aim:

- A robust nonlinear model predictive controller needs to be synthesised, which explicitly takes model uncertainty into consideration during controller synthesis. The objectives stated in Section 1.2 should be included in the objective function of the controller.
- The controller should be verified through a simulation study of the closed-loop system in order to evaluate the performance of the controller :
 - in the presence of uncertainty about the feed ore hardness and feed ore size distribution, and
 - disturbances such as spillage water being added to the sump.
- The performance of the RN MPC is compared to a nominal nonlinear model predictive controller and single-loop PI controllers to gauge the advantages of using robust nonlinear model predictive control.

This dissertation contributes the following:

- Mill model in the form required for control.
- Linearised models of the nonlinear model for tuning the PI controllers.
- Synthesis of PI controllers with anti-windup for the ROM ore milling circuit.



- Synthesis of a nonlinear model predictive controller (one that does not take model uncertainty into account) for the ROM ore milling circuit.
- Synthesis of an *open-loop* robust nonlinear model predictive controller for the ROM ore milling circuit. Open-loop model predictive control differs from closed-loop model predictive control in assuming that there is no feedback over the prediction horizon during the prediction and optimisation calculations. This therefore leads to more divergent state trajectories during prediction and optimisation when disturbances and uncertainties are present in open-loop formulations compared to closed-loop formulations, resulting in controllers with more conservative performance and with smaller feasibility regions.
- Simulation study to compare the stability and performance of the above-mentioned controllers under model mismatch situations
 - using severe parameter uncertainty with a uniform distribution and zero mean to establish a baseline,
 - adding a large step change that increases the feed ore hardness and drives some variables to their constraints,
 - adding a large step change in the feed ore size distribution that increases the number of large particles in the feed, and
 - adding a disturbance to the sump by adding a step increase to the sump feed water that simulates spillage water being added to the sump.

1.4 ORGANISATION

Chapter 2 provides a brief overview of the ROM ore milling circuit process and an overview of the modelling of the main process units in the ore milling circuit such as the mill and the cyclone.

Chapter 3 provides an overview of the theory of stability of MPC and the development of the RN MPC theory. The chapter continues by taking an in-depth look at the RN MPC formulation.

Chapter 4 outlines the theory of the single-loop PI controllers with anti-windup, Skogestad Internal Model Control (SIMC) tuning method and the application of the theory to the linearised process models of Section 4.3 to synthesise the PI controllers.

Chapter 5 provides an in-depth study of the robust and nominal nonlinear model predictive controllers as well as the single-loop PI controllers applied to the nonlinear model of the ROM ore milling circuit. Practical scenarios are investigated in an attempt to quantify the



effects of severe feed ore disturbances and parameter variations on the closed-loop performance.

Chapter 6 provides a short summary of the thesis, some conclusions drawn from the simulation studies and recommendations for further work regarding the development of an RN MPC for the ROM ore milling circuit.

Addendum A outlines the technical details related to the software implementation of the RN MPC control algorithm.

Addendum B shows some additional results relating to simulation scenarios described in Chapter 5 as well as simulation results for additional scenarios that were not covered in Chapter 5.

Addendum D provides a table that summarises the simulation results of both Chapter 5 and Addendum B.

CHAPTER 2

MILLING THEORY AND MODELLING

2.1 INTRODUCTION

Controlling a process usually requires a mathematical model of the process for design and simulation purposes. Model-based control further relies on an internal model of the process to calculate the control moves. A mathematical model of the ROM ore milling circuit is therefore essential in designing and simulating control strategies. There are two approaches to modelling grinding circuits, firstly a process design and optimisation approach and secondly a control and estimation approach.

Process engineers want as much information as possible about the operation of the mill and grinding circuit as a whole. Simulation models provide insights into the mechanisms of breakage and material flow inside the mill (Hinde, 2007). The simulation models consist of a large number of states and parameters in order to model the size distributions and breakage distributions.

Control engineers have only limited measurements available from the mill and circuit (Apelt *et al.*, 2002), that limit the number of states and parameters that can be estimated. Control engineers therefore prefer simple models with only a small number of states and parameters, while still capturing the essential dynamics for control purposes.

2.2 THEORY OF MILLING

2.2.1 Introduction

Milling or grinding reduces the size of ore by allowing the ore to tumble freely in a rotating or gyrating container, which causes a breaking action to be applied to the ore. The product

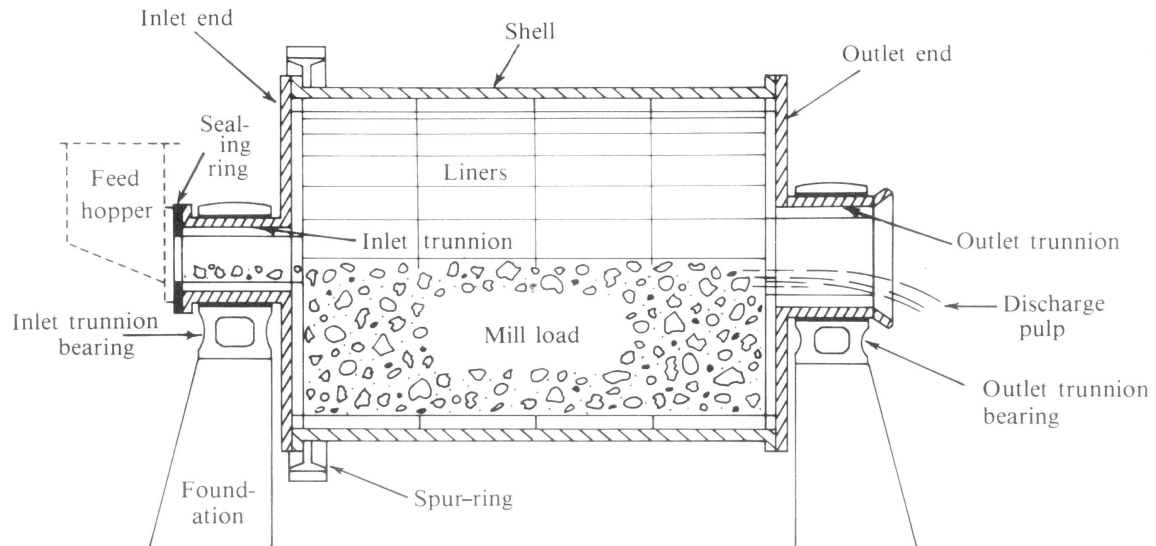


Figure 2.1: Mill Schematic (Stanley, 1987).

size is determined by the size of the feed to the mill and by relative probabilities of breakage of the individual size fractions inside the mill (Stanley, 1987).

In gold ores, the valuable gold usually constitutes a very small part of the volume of the ore. The rest of the ore is mostly worthless. In order to extract the gold from the ore, the ore has to be ground down to a fine powder. This action or process of reducing the size of ore to minute particles or fractions is called comminution (Stanley, 1987).

Comminuting ore therefore

- makes it more usable because of the reduced particle size, and
- liberates the different components in the ore from each other, which aids in the subsequent separation of the components by down-stream processes.

The separation of the valuable material from the gangue, or worthless material, is achieved through chemical or physical mineral recovery processes. It is reasonable to assume that the closer the maximum discharge particle size from the milling process is to the grain size of the valuable material, the more efficient the downstream recovery processes will be, because the valuable material will be better liberated from the ore (Stanley, 1987).

The desired fineness of the particle size obtained from the milling process is also determined by the economics of the process. The gain in recovery is weighed against the cost of finer comminution (Stanley, 1987).

2.2.1.1 Mills

Tumbling mills are usually cylindrically shaped machines made of steel (Figure 2.1). The cylindrical container is rotated about its horizontal axis by some form of drive, usually elec-



trical. Both ends of the cylinder are closed off with either cast iron or steel, with the centres of the ends extruding to form hollow trunnions that allow ore to enter the mill and pulp to exit. The trunnions are supported by trunnion bearings that allow the mill to rotate, while the bearings are mounted on some form of foundation (Stanley, 1987).

The ore enters the mill through the inlet trunnion by some form of feeder, which is a device that can continuously feed ore into the inlet trunnion from external sources. It can be a static device that allows the ore to flow by means of gravity (such as sprout and hopper feeders) or it may be attached to the mill that allows it to rotate and scoop the feed ore into the inlet trunnion (such as scoop and drum feeders) (Stanley, 1987).

The inside surfaces of the mill are protected against wear by mill liners. The mill liners are important for two reasons. Firstly, the mill liners are consumables that influence the operational cost of the mill, because they wear away over time. The operational costs associated with mill liners can be minimised by maximising the time before the liners need to be replaced, as well as minimising the cost of relining. Secondly, it is partly responsible for the effectiveness of the mill. The shell liners have different shapes that aid in lifting the ore and thus transferring energy to the ore for grinding. Ensuring that the lifters remain efficient over the lifetime of the liners is therefore also important (Chandramohan and Powell, 2006, McBride and Powell, 2006).

The pulp exits the mill through the outlet trunnion and there are several methods to facilitate this. There is a simple overflow mill (Figure 2.1) where the pulp overflows into the outlet trunnion aided by the rotation of the mill. Secondly, a screen-and-discharge mechanism can be employed, where the pulp passes through a screen that limits the particle size to the screen aperture size and lifter bars lift the pulp to the outlet trunnion (Figure 2.2). A peripheral discharge and open-ended discharge can also be employed to eliminate the need for lifting pulp through the outlet trunnion. The peripheral discharge (Figure 2.3) consists of grates on the side of the mill at the outlet end through which the pulp flows. With an open-ended discharge, the mill outlet end is not closed off by a solid side, but rather by a screen or grate, that allows pulp to exit through the whole outlet opening. The open-ended mill cannot be supported by an outlet trunnion, but rather by a roller system (Figure 2.4) or slipper bearing (Figure 2.5) (Stanley, 1987). The different discharge mechanisms influence the performance of the mill. If a slurry pool forms inside the mill, the grinding performance is degraded (Latchireddi and Morrell, 2003a, b).

There are different mill types:

Ball Mills use steel balls ranging from 100 mm down to 50 mm as grinding medium. Their primary role is for primary milling after crushing if the run-of-mine material has insufficiently sized pebbles to support autogenous milling.

Rod Mills use steel rods with diameters of about 100 mm and a length that is about 100 mm shorter than the length of the mill. Rod mills can handle coarser material than other

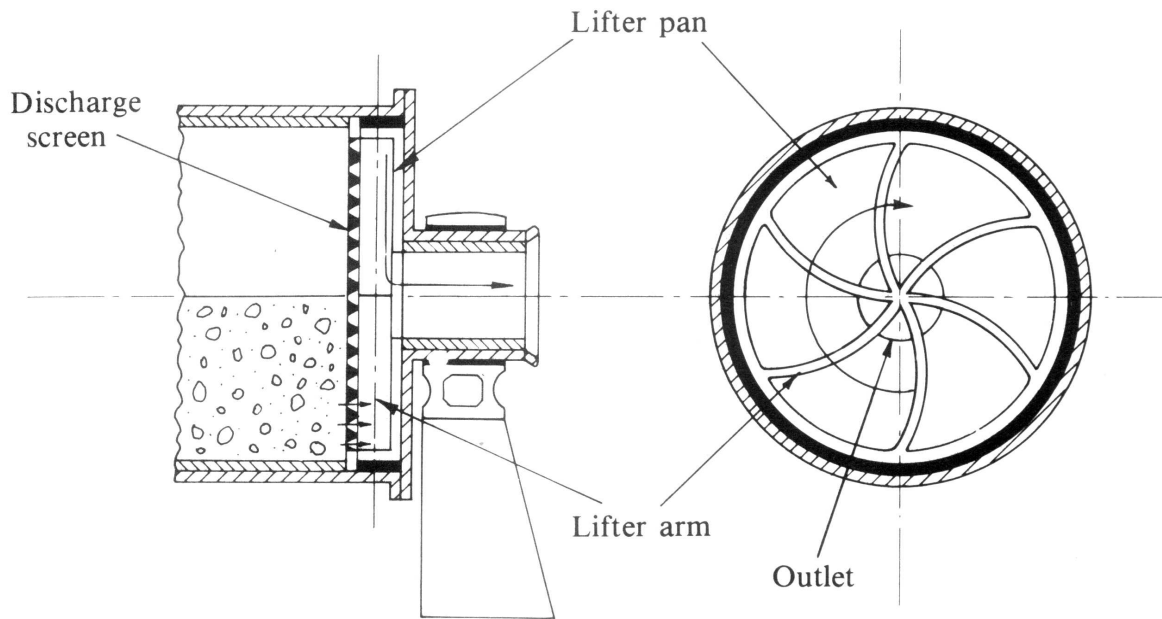


Figure 2.2: Mill Discharge - Pulp and lifter (Stanley, 1987).

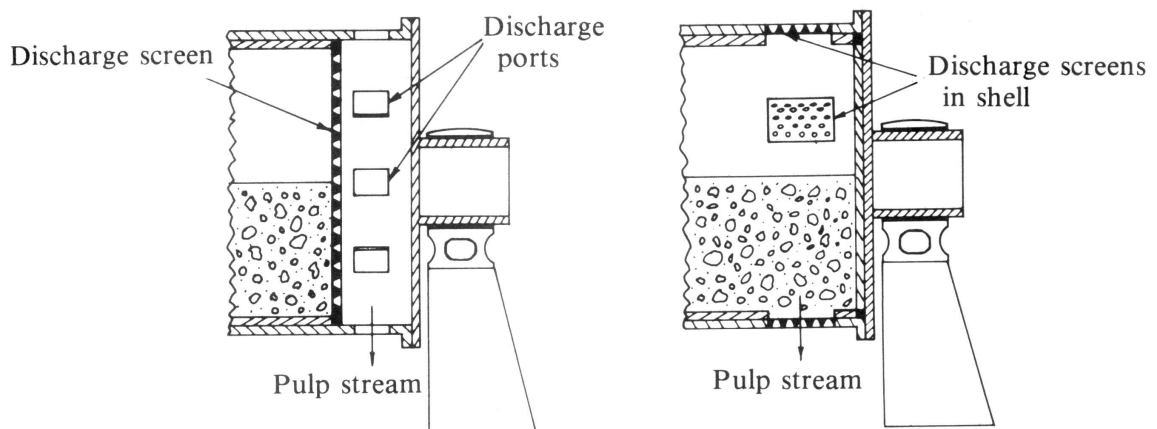


Figure 2.3: Mill Discharge - Peripheral discharge (Stanley, 1987).

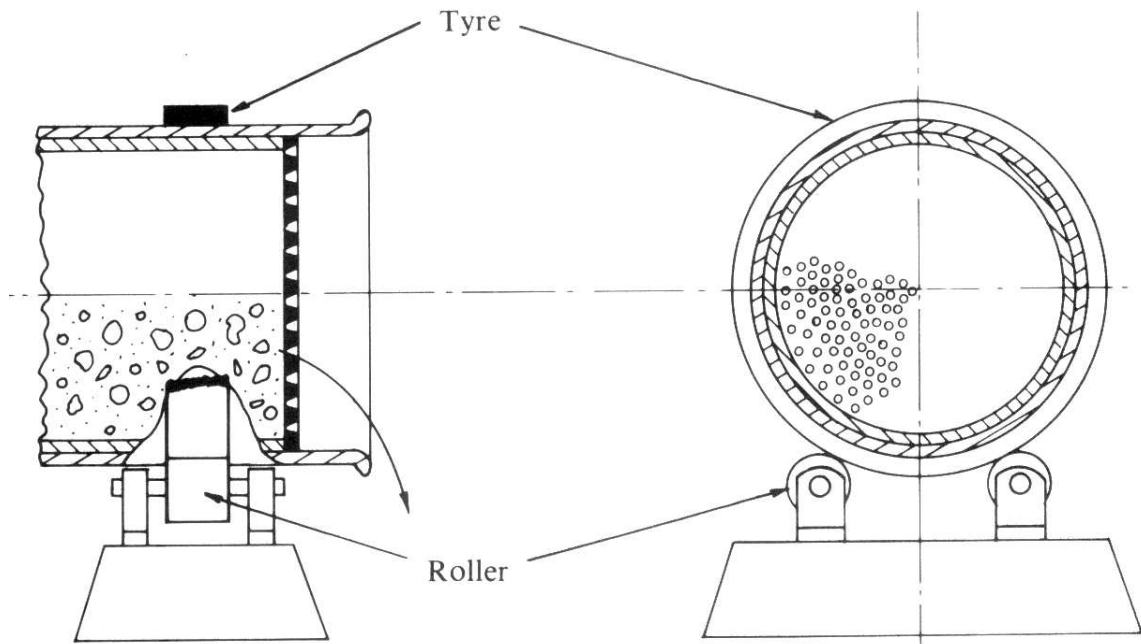


Figure 2.4: Mill Discharge - Open-ended discharge with roller and tyre (Stanley, 1987).

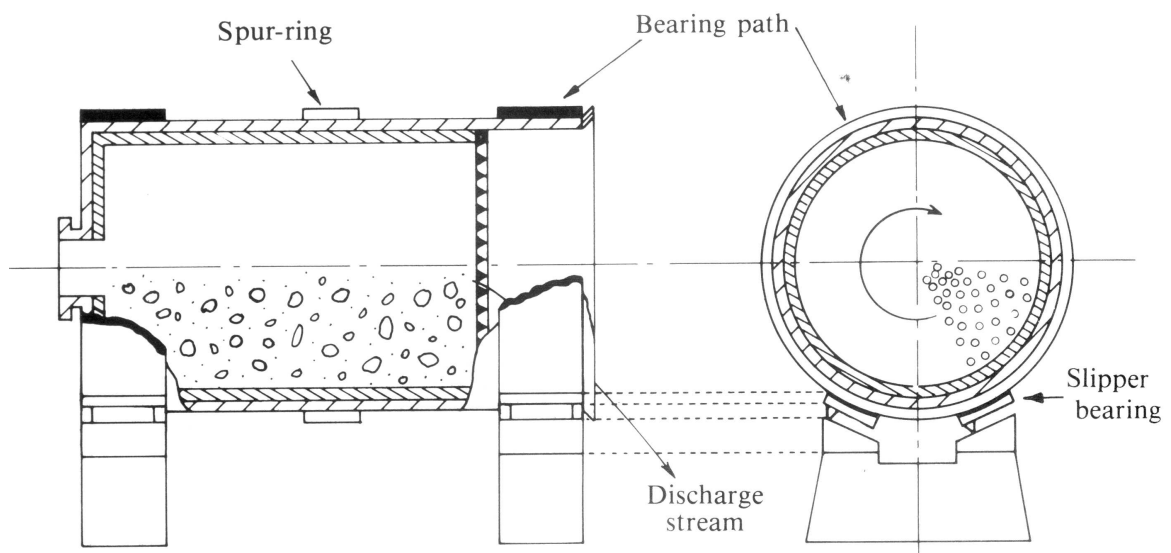


Figure 2.5: Mill Discharge - Open-ended discharge with slipper bearing (Stanley, 1987).

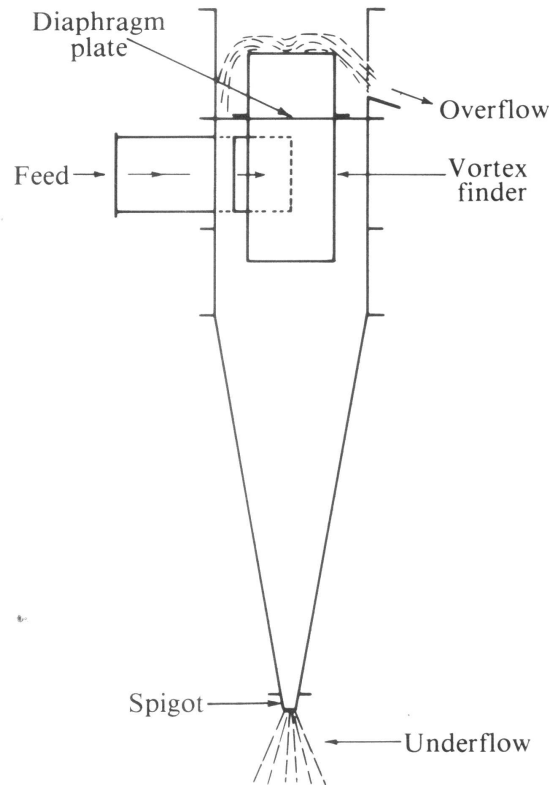


Figure 2.6: Hydrocyclone schematic (Stanley, 1987).

types of milling and produce finer particles than crushing, and are therefore ideal as intermediary between crushing and other types of milling.

Autogenous Mills use only the ore as grinding medium. There are two types of autogenous (AG) mills. The first type uses the ROM ore directly as grinding medium and is only suitable for primary milling. The advantage is that no crushing is required, except for very large pieces to facilitate handling. The second type uses pebbles rather than balls or rods as grinding medium and is therefore suitable for any stage of milling.

Semi-autogenous Mills use steel balls together with ore as grinding medium. The power draw of the mill is a function of the bulk density of the load. The bulk density of AG mills is lower than that of same-sized ball and rod mills, which affects the power draw and the grinding capacity of the AG mills. The AG mills have to be larger than ball or rod mills to have the same grinding capacity. The SAG mills increase the bulk density of the mill compared to AG mills and therefore have increased grinding capacity for the same size as AG mills. SAG mills can still be used to grind run-of-mine ores.

2.2.1.2 Hydrocyclones

Hydrocyclones (Figure 2.6) are centrifugal classifiers. They work by injecting a feed slurry tangentially into the cylindrical section of the device. The centrifugal forces that result force



the solid particles through the suspended water to the cylinder wall. The particles experience drag forces as they move through the suspended water, causing heavier material to move preferentially to the cylinder walls, while lighter material does not move all the way to the cylinder wall. Most of the liquid is forced to the centre of the device owing to displacement taking place. The liquid together with the lighter material is ejected through the central vortex finder to the overflow. The heavier particles are displaced by newer particles entering the device that cause axial as well as tangential forces. The heavier particles cannot escape at the overflow, because they are stopped by the diaphragm and forced to the conical section where they are guided to the underflow opening or spigot. The cut size of the cyclone is highly dependent on the feed density and less on the cyclone dimensions. The cyclone cut can therefore be controlled by changing the feed density to the cyclone (Stanley, 1987).

2.2.1.3 Sump

The mill usually discharges into a sump from the top, where extra water is added to dilute the pulp. The sump acts as a buffer to disturbances in the feed to the cyclone. In smaller sumps, the pulp is assumed to be fully mixed, while in bigger sumps some settling may occur that could affect the discharge density at the bottom of the sump (Hulbert, 2005).

2.2.2 Process of breakage

Most comminution processes apply compression to ore particles. Elastic bodies distort when compressed by flattening in the direction of compression and bulging at right angles to the compression force. This bulging of the particle induces tensile stresses inside the particle. The tensile stresses are concentrated at the edges of flaws in the particles. The greater the flaw area is, the greater the concentration of force. If the tensile stress at the flaw edges reaches a critical value, the intermolecular bonds break. As the bonds break, the area of the flaw increases and the concentration of force at the edge of the flaw is increased, which causes more molecular bonds to break. The flaw is almost instantaneously converted to a crack. As the crack propagates, other flaws are activated and start to crack. This results in the particle being covered in a network of cracks that divide it into roughly equal fragments (Kelly and Spottiswood, 1990, Stanley, 1987).

The crack directs compressive strain energy in equal amounts to the two parts on either side of it. If the energy is sufficiently large, it can cause the pieces to break further. The two fragments are unlikely to be equally large in terms of mass, and the smaller fragment is therefore more likely to break owing to the greater energy per mass concentration of that fragment. The breakage process is concentrated on smaller and smaller particles. Every time a fragment splits, the energy is divided between the fragments, with the smaller fragment being more likely to break, until the energy levels fall below the threshold to support further breakage (Kelly and Spottiswood, 1990, Stanley, 1987).



The comminution process needs to apply enough energy to reach the critical level to cause the initial crack network to form. Once breakage starts to occur, most of the energy is then converted to heat in the form of vibrations within the particle fragments (Kelly and Spottiswood, 1990, Stanley, 1987).

2.2.2.1 Size distribution

Brittle fracture breakage produces a product with a spread of differently sized fragments. This final product consists of a particle distribution, where this distribution is an important factor in the efficiency of further processing. Determining this size distribution is done by sieving a sample of the final product. The aperture area of each successive sieve is half that of the previous sieve (Stanley, 1987). The sieve apertures are usually square and the size is expressed as the length of one of the aperture sides. The size distribution of the final product is expressed in discrete sizes by either stating

- the *differential distribution*, which is the percentage of the total sample mass in each size fraction in decreasing aperture sizes, or
- the *cumulative distribution*, which is defined as the combined mass of all the size classes starting from either the coarsest or the finest sieve to the sieve in question and expressing that mass as a percentage of the total sample mass.

The cumulative distribution is more commonly used to express the particle size distribution. The *size fraction* is defined as the amount of material between two successive sieves as a fraction of the total sample mass. For routine plant control the total size distribution is not required, but only the proportion passing or being retained by a certain sieve size, which is typically $75\mu\text{m}$ (Hulbert, 2005, Stanley, 1987).

2.2.3 Motion of the load

The contents of the mill or *load* consist of a mixture of grinding media and pulp that fills less than half the volume of the mill. The grinding media can either be balls or rods or pieces of rock called pebbles, depending on the type of mill. When the mill is at rest, the load lies at the bottom of the mill. When the mill starts to rotate, the load is lifted on the rising side of the mill to a height determined by the speed of the mill and the slip between the mill shell and the load (Stanley, 1987).

If the height is low when the materials reach the top of their travel, the load will curve over, slide and roll down the rising portion of the load until it reaches the bottom of the mill. This motion is called *cascading* (Stanley, 1987).

If the speed of the mill is sufficiently fast, the material in the load will be projected airborne after reaching the top of its travel on the mill shell. The uppermost point where the charge



leaves the mill shell is defined as the *shoulder* (Powell and McBride, 2004). After becoming airborne, the particles will rise some more before falling back, following parabolic paths. The highest vertical point that the airborne particles reach is defined as the *head* (Powell and McBride, 2004). The particles will be mostly out of contact while in the air. The area where the particles make contact with the mill after being airborne is called the *impact toe* of the mill (Powell and McBride, 2004). This motion is called *cataracting* (Powell and McBride, 2004, Stanley, 1987).

There is high energy in the *impact toe* zone of the mill where most of the breakage occurs. There is relative motion between successive layers of the rising load. The slip occurring between layers causes additional breakage to occur through a process called attrition that is present from low rotational speeds up to high rotational speeds (Powell and McBride, 2004, Stanley, 1987).

If the rotational speed of the mill becomes sufficiently high, the centrifugal force acting on the outer layer of the load will overcome the centripetal component of the weight. At this point the grinding medium will stay connected to the mill shell for the whole rotation of the mill. This motion is described as *centrifuging*. In this state, very little grinding takes place in the mill. The speed at which this starts to occur is called the *critical speed* of the mill and can be calculated as

$$N_{\text{critical}} = \frac{42.23}{\sqrt{\text{Mill}_{\text{Diameter}}}} \quad (2.1)$$

where $\text{Mill}_{\text{Diameter}}$ is the inside diameter of the mill in metres, taking the mill liners into account and N_{critical} is the critical speed of the mill in revolutions per minute (RPM). (Stanley, 1987).

2.2.4 Forces causing breakage

Inside a mill, there are three types of forces that can cause breakage (Stanley, 1987):

- *Impact* forces occur when a particle is hit by another particle with high momentum. The particles can hit other particles or the mill shell. Impact energy is typically highest in the toe of the load, where most of the airborne particles make contact with the load.
- *Compression* forces are exerted where particles are trapped between other particles or against the mill shell and squeezed. This usually occurs at the bottom of the mill where the load is tightly packed.
- *Shear* forces occur where the layers of the load slide across each other with pressure. These forces occur mostly in the rising area of the load and in slowly rotating mills occur in the descending portion of the load as well.



2.2.5 Breakage mechanisms

The forces in the previous subsection do not necessarily result in breakage. If the forces are below the threshold required, no breakage will occur or only partial breakage will occur (Shi and Kojovic, 2007).

The threshold energy is also dependent on the size of the particle. The larger the particle, the more faults it contains and the weaker it becomes and therefore less energy is required to break it (Yashima *et al.*, 1987).

Partial breakage or *attrition* breakage can be subdivided into two types:

- Abrasion breakage (Loveday and Naidoo, 1997, Loveday *et al.*, 2006), which involves breaking away a part of the particle surface as a flake or even small particles.
- Chipping, which is the corner of an edge of the particle breaking away.

Both these breakage mechanisms occur when the forces are not large enough to cause the whole particle to shatter. Attrition breakage therefore causes bimodal size distribution to occur, because the main particle remains almost the same size with only some small fragments forming owing to the breakage (Stanley, 1987).

The third breakage mechanism is called true impact breakage and occurs when the particle is sufficiently stressed to the point where it shatters completely (Stanley, 1987).

2.3 MILLING MODELLING

Simulation of the mill operation is important to determine the mechanisms of breakage and the conditions affecting it. Better understanding of the charge behaviour will lead to optimising the level of grinding and maximising the capacity of the milling circuit. Measurement of the breakage mechanisms and charge behaviour inside the mill is impractical, because there are currently no online sensors that can withstand the harsh environment inside the mill (Mishra, 2003a).

Milling is not a very efficient process (Cleary, 2001, Kapakyulu and Moys, 2007) and better understanding of the mode and mechanisms of energy utilisation in the milling process through simulation can help increase the efficiency of milling (Mishra, 2003a).

Mill modelling research is divided into two main categories. Firstly the newer trend is to model the individual particles inside the mill using a discrete element method (DEM) (Mishra, 2003a, b) and secondly the mill model is based on mass balance models (Bazin *et al.*, 2005, Morrell, 2004a).

There are many papers in the field of mill modelling and this section gives a brief overview of the main results. This is by no means intended to be an exhaustive review of the available literature, as the focus of this thesis is the application of advanced control to a milling circuit.



2.3.1 Discrete element method

DEM modelling gives comminution researchers better insight into the breakage mechanisms taking place inside the mill. DEM allows the individual collisions between the constituents in the mill to be modelled and when this is applied to the entire mass of charge inside the mill, gives insight into the overall charge motion and behaviour (Mishra, 2003a). The discrete element method is making a significant contribution in analysing the elementary processes involved in grinding particles where impact geometries and other local environmental factors are very important (Mishra, 2003b).

The DEM could provide information on the interactions between particles, especially on how the collision energy is distributed between impact and abrasion, using energy distributions rather than average energy in the mill and using ore characteristics determined by impact and abrasion tests to predict particle breakage based on the energies applied as a result of particle interaction and size. There is still a need for research to couple the material motion and interactions to breakage tests in order to simulate breakage inside the mill reliably (Powell and McBride, 2006). The JKDrop Weight Tester characterises ores for predicting single event breakage caused by impact. Breakage in tumbling mills occurs as a result of several different modes of breakage and involves multiple events. It proves difficult to link the different modes of breakage to the motion of the particles in DEM (Morrison *et al.*, 2006).

Research in DEM focuses on understanding the contact between particles and the mechanisms of breakage (Chandramohan and Powell, 2005, Cleary, 2001, Djordjevic *et al.*, 2006, Morrison *et al.*, 2006, Morrison and Cleary, 2004, Morrison *et al.*, 2007). The development of a contact law for describing the collisions between particles and their environment is essential to properly describe the motion of particles inside the mill and any boundary objects with which they interact (Cleary, 2001).

DEM can better describe the charge motion inside the mill and the influence of different operating conditions on the charge motion and the effectiveness of grinding (Powell and McBride, 2004). By adding smoothed particle hydrodynamics (SPH), slurry effects such as lifters crashing into slurry pools, fluid draining from lifters, flow through grates and pulp lifter discharge can be modelled. The dynamics of slurry inside the mill can therefore be studied with respect to operating conditions, slurry viscosity and slurry volume (Cleary *et al.*, 2006).

DEM can be used to predict the power draw of the mill more accurately (Abd El-Rahman *et al.*, 2001, Djordjevic, 2005). Empirical models are reliable in predicting power draw, but are limited to mills and operating conditions that fall within the model database boundaries and cannot model the impact that the changing conditions inside the mill have on power draw, because of their static nature (Djordjevic, 2005).

Simulation of liner wear inside the mill can greatly assist in designing industrial mills. The effect of lifter wear on charge behaviour can aid in optimising grinding over the lifespan of



the lifters from an operational viewpoint as well as maximise lifter lifespan from a design viewpoint (McBride and Powell, 2006).

Similar to DEM for mills, hydrocyclones are modelled by capturing the fundamentals through computational fluid dynamics (Nageswararao *et al.*, 2004). In the short term this approach will result in optimisation of cyclone design and in the longer term it will provide more accurate simulation and control of hydrocyclones.

The DEM still faces a big hurdle for control purposes. The models are very computationally expensive and currently cannot be used for real-time simulation. It will take some time for the computational power to increase sufficiently to use DEM models for real-time simulation and control. For the time being, a hybrid approach might be employed where empirical models are developed with the aid of computationally intensive models such as DEM for mills and computational fluid dynamics for hydrocyclones (Djordjevic, 2005, Nageswararao *et al.*, 2004).

2.3.2 Population balance models

Modelling of mills, especially SAG/AG mills, can be described in terms of a population balance and perfectly mixed reactor (Whiten, 1974). The model of size-by-size solids mass balance is based on the following equation (Apelt *et al.*, 2002, Morrell, 2004a) developed by the Julius Kruttschnitt Mineral Research Centre (JKMRC)

$$\text{Accumulation} = \text{In} - \text{Out} + \text{Generation} - \text{Consumption} \quad (2.2)$$

$$\frac{\partial s_i}{\partial t} = f_i - p_i + \sum_{j=1}^{i-1} r_j s_j a_{ij} - (1 - a_{ii}) r_i s_i \quad (2.3)$$

where

f_i	feedrate of particles of size class i [tph]
p_i	discharge rate of particles of size class i [tph]
r_i	breakage rate of particles of size i [hr^{-1}]
s_i	mass of particles in the charge of size i [tons]
a_{ij}	appearance function of particles in size i (describes the amount of material “selected” for breakage and the distribution of material after breakage occurred) [fraction]

The model describes the inflow of particles in each size class (f_i), the outflow of particles in each size class (p_i), the generation of material in the current size class i by breakage of material in the larger size classes j down to the current size class i , consumption of material in the current size class i by breakage down to smaller size classes and holdup of solids in size class i (s_i).



The model of water mass balance is based on the following equation (Apelt *et al.*, 2002)

$$\text{Accumulation} = \text{Inflow} - \text{Outflow} \quad (2.4)$$

$$\frac{\partial s_w}{\partial t} = f_w - p_w \quad (2.5)$$

where

f_w	feedrate of water [tph]
p_w	discharge rate of water [tph]
s_w	mass of water [tons]

The model describe the inflow of water (f_w), the outflow of water (p_w) and the holdup of water in the mill (s_w).

The advantage of this model is its simplicity, but this is the source of its greatest disadvantage as well. The model has no physical description of the sub-process of breakage and discharge. To make this model useful, models for the various sub-processes need to be defined.

2.3.2.1 Product discharge

The solids product p_i that is discharged from the mill is calculated as follows (Apelt *et al.*, 2002):

$$p_i = d_0 c_i s_i \quad (2.6)$$

where

p_i	discharge rate of product in size class i [tph]
d_0	maximum mill discharge rate constant [hr^{-1}]
c_i	grate classification function for size class i (probability of particle passing through discharge grate) [fraction]
s_i	mass of particles in the charge of size i [tons]

and water discharging from the mill is calculated as follows (Apelt *et al.*, 2002):

$$p_w = d_0 s_w \quad (2.7)$$

where

p_w	discharge rate of water [tph]
d_0	maximum mill discharge rate constant [hr^{-1}]
s_w	mass of water inside the mill [tons]

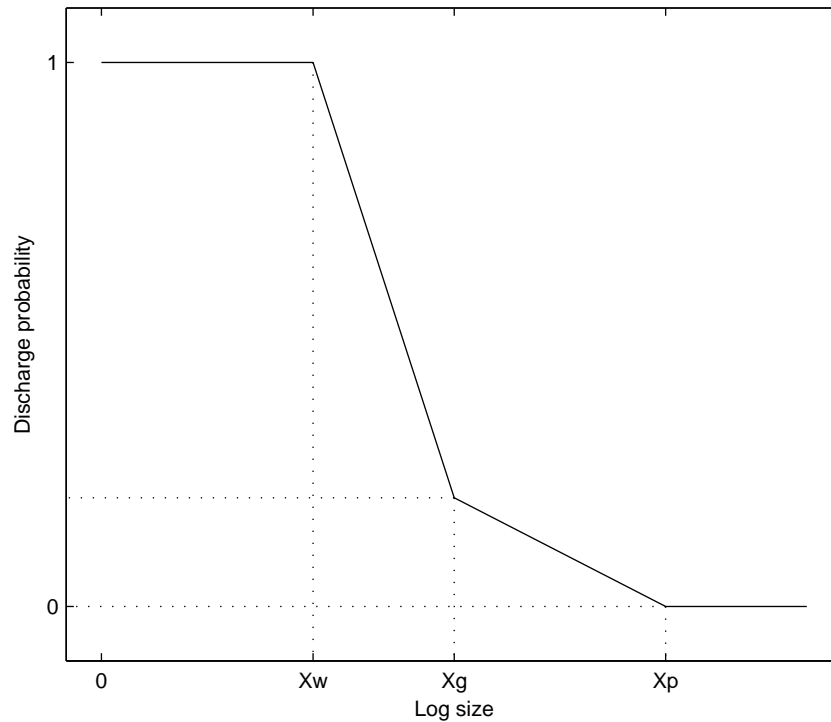


Figure 2.7: Grate classification function as in Morrell (2004a)

The grate classification function c_i describes the discharge behaviour of each size class through the discharge grate. It is defined as the probability of each size class passing through the grate. Particle sizes larger than the grate aperture size x_p have a discharge probability of zero. Small particle sizes that behave like water ($x < x_w$) have a discharge probability of one. The particle size classes x_i that lie between the water-like size and grate aperture size ($x_w < x_i < x_p$) show a linear decrease in discharge probability (Morrell, 2004a) or more complex probability curves (Amestica *et al.*, 1993, 1996).

A model is needed to describe the grate classification c_i and the maximum discharge value d_0 in equation (2.6). Development of a model to take advantage of the constant discharge seen for particles that are water-like ($x < x_w$) of the form seen in Figure 2.7 was done by Morrell and Stephenson (1996) by taking into consideration the effects of grate design, mill speed and charge volume. The work was later extended by doing an extensive laboratory study on the effects of pulp lifters and grate designs (Latchireddi and Morrell, 2003a, b).

Amestica *et al.* (1993) found that there is an increase in discharge in material just smaller than the effective grate size x_p that can be explained as the combination of two classification actions. The first classification action is larger dry material being thrown through the grate and the second action is the result of material being carried in the slurry percolating through the bed packed against the grate.

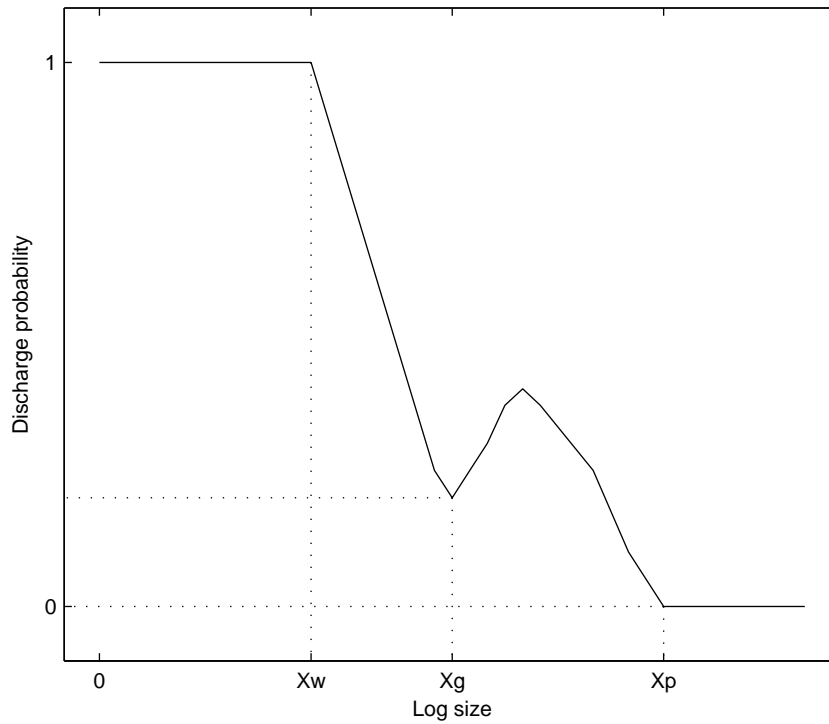


Figure 2.8: Grate classification function as in Amestica *et al.* (1996)

2.3.2.2 Breakage rate r_i

The breakage rate model or “variable rates model” (Morrell, 2004a, Morrell and Morrison, 1996) describes the fraction of material in each size class that is “selected” for breakage. The larger size classes usually have a larger percentage selected for breakage than the smaller size classes. The “variable rates model” extends the breakage rate model by varying the fraction selected for breakage for each size class according to the breakage conditions inside the mill. The breakage rate curve can be described in terms of cubic splines. The cubic splines are described by so-called “knots” with associated base breakage values (Morrell, 2004a, Morrell and Morrison, 1996). The values between the knots are calculated by interpolation. The equations describing the base breakage rates for the knot points are as follows:

$$\ln(R_i) = k_{i1} + k_{i2}J_b D_b + k_{i3}\omega + k_{i4}J_t \quad (2.8)$$

where

- R_i breakage rate values for rates $i = 1 - 5$ [hr^{-1}].
- J_b volume of balls inside the mill [percentage].
- J_t volume of mill filled by grinding media (balls and rocks) [percentage].
- D_b make-up ball size.
- ω mill rotational rate.
- $k_{i1} - k_{i4}$ constants for rates $i = 1 - 5$.



The effects of ball load, ball size, total load and speed on the breakage rate distribution were studied (Morrell, 2004a) as well as feed size distribution and recycle load (Morrell and Morrison, 1996). The difference between pilot plants and full-scale plant breakage rate distributions was also investigated (Morrell, 2004a) and the differences observed can be attributed to the higher rotational speed in pilot plants compared to full scale plants for the same fraction of critical speed. This is due to the differences in mill diameter (Morrell, 2004a) and should be included in the breakage rate models as a correction factor for scale-up from pilot plants to full-scale plants.

2.3.2.3 Breakage distribution function (appearance function a_{ij})

The appearance function a_{ij} of equation (2.3) is a matrix describing the *breakage* and the distribution that results after breakage, thus the breakage distribution (Apelt, 2002), for the material “selected” for breakage by the breakage rate function r_i (Section 2.3.2.2).

The breakage distribution function describes the distribution of smaller rock fragments that form when rock fragments in each size class breaks. This distribution is dependent on the hardness of the rock and the energy that is applied to break it. The function that describes the breakage distribution will therefore be ore-specific and related to the energy applied to break it (Morrell, 2004a). The breakage distribution function is the weighted average of two breakage processes; the first process is shatter at high energy intensities and the second process cleavage at low energy intensities. In mills, both these breakage processes are at work at the same time and the smaller rock fractions may break even further (Kelly and Spottiswood, 1990).

The breakage distribution function as used by the JKMRC (Morrell, 2004a) can be summarised as:

$$t_{10} = A \left(1 - e^{-b \cdot E_{cs}} \right) \quad (2.9)$$

where A and b are ore-specific and E_{cs} relates to the impact energy to give a size distribution index t_{10} . The characterisation of A and b is done through drop-weight tests for different ores (Napier-Munn *et al.*, 1996). The size distribution index t_{10} can then be related to a size distribution (Narayanan and Whiten, 1988).

Recent research shows that more energy is needed to break smaller particles than larger particles (Tavares and King, 1998). This was confirmed by Banini (2000) who conducted drop-weight tests on eight mineralised ore types from gold, copper and lead/zinc ore to quarry material. Fitting average characteristic A and b values for small to large particles leads to questionable performance in mills that have particles from 200 mm down to minus 1 mm (Shi and Kojovic, 2007). Shi and Kojovic (2007) fitted a modified version of a model developed by Vogel and Peukert (2003, 2005) to the drop-weight test data conducted by Banini (2000). The modified model explicitly incorporates particle size into the equation



together with material properties and cumulative impact energy as follows:

$$t_{10} = M \left\{ 1 - e^{-f_{mat} \cdot x \cdot k \cdot (E_{cs} - E_{min})} \right\} \quad (2.10)$$

where

t_{10}	cumulative percentage passing 1/10 of the initial size [percentage].
M	maximum t_{10} for a material subject to breakage [percentage].
f_{mat}	material-specific breakage characteristic [dimensionless].
x	size of the particles [m].
E_{cs}	mass-specific impact energy [$\frac{J}{kg}$].
E_{min}	threshold energy needed before breakage occurs or accumulates [$\frac{J}{kg}$].

The modified breakage distribution function in equation (2.10) can be related to the breakage distribution function in equation (2.9), because M is equal to A , $f_{mat} \cdot x$ to b , and $k(E_{cs} - E_{min})$ to E_{cs} . The modified breakage distribution function (2.10) describes material with three property parameters (f_{mat} , x the particle size and threshold energy E_{cs}), which makes it more flexible than (2.9). Shi and Kojovic (2007) concluded that the modified breakage distribution function fitted the test data well, while requiring only one set of parameters for each ore type, and has a fundamentally better structure for describing the effect of particle size on the breakage distribution function.

Experimental procedures are necessary to obtain the breakage distribution so that it can be fitted to the models (2.9)-(2.10) given above. There are a number of methods to obtain the breakage distribution by single impact energy. There is the dual pendulum method (Narayanan, 1987) and the ultrafast load cell method (King and Bourgeois, 1993, Tavares and King, 1998). A batch grinding test can also be used to determine the breakage distribution function (Austin and Luckie, 1972, Austin and Bhatia, 1972).

2.3.2.4 Power draw model

The mill power model uses the holdup of rock and quantity of slurry in the mill to predict the volume, density and position of the charge in the mill (Morrell, 2004a). By conducting an energy balance around the mill and assuming that power is the tempo at which potential and kinetic energy is applied to the charge, the power draw of the cylindrical ($P_{cylinder}$) and conical (P_{cone}) sections of the mill can be expressed as (Morrell, 2004a)

$$P_{cylinder} = \int_{r_i}^{r_m} V_r L r g (\rho_c (\sin \theta_s - \sin \theta_t)) + \rho_p (\sin \theta_s - \sin \theta_{tp}) dr \quad (2.11)$$

$$P_{cone} = \int_0^{L_i} \int_{r_i}^{r_c} V_r r g (\rho_c (\sin \theta_s - \sin \theta_t)) + \rho_p (\sin \theta_s - \sin \theta_{tp}) dr dL_c \quad (2.12)$$



where

L_c	The length of the cone-end, measured from the cylindrical section, at a radius of r_c [hr^{-1}].
L_i	The length of the charge surface within the cone ends [percentage].
L	The length of the cylindrical section of the mill inside the liners [percentage].
P	The power delivered to the charge (net power).
r	The radial position.
r_i	The radial position of the inner surface of the charge.
r_m	The radius of the mill inside the liners.
r_c	The radius of the cone-end of the mill at a distance of L_c from the cylindrical section of the mill [metres].
V_r	The tangential velocity of a particle at radial distance r from the centre of the mill.
θ_s	The angular displacement of the charge shoulder position at the mill shell.
θ_t	The angular displacement of the charge toe position at the mill shell.
θ_{tp}	The angular displacement of the slurry toe position at the mill shell.
ρ_c	The density of rock and ball charge (excluding the pulp).
ρ_p	The density of the pulp phase.

The power equations (2.11) and (2.12) describe the energy applied to the charge and exclude electrical and mechanical losses. A further equation is needed to describe the power draw that includes the losses to calculate the gross power draw of the mill. The no-load power equation developed by Morrell (1996) and summarised by Apelt *et al.* (2001) is given by:

$$P_{gross} = P_{No-Load} + kP_{Charge} \quad (2.13)$$

where

P_{gross}	The mill power [kW].
$P_{No-Load}$	The no-load or empty mill power draw [kW].
P_{charge}	The net power applied to the charge of the mill [kW].
k	The lumped parameter of all losses [dimensionless].



The no-load component of equation (2.13) is given by (Apelt *et al.*, 2001)

$$P_{No-Load} = 1.68 \left(D_m^{2.5} \phi_{fcs} (0.677L_{cone} + L_m) \right)^{0.82} \quad (2.14)$$

where

$P_{No-Load}$	The no-load or empty mill power draw [kW].
D_m	The mill inside diameter [metres].
ϕ_{fcs}	The mill speed as a fraction of critical speed [fraction].
L_{cone}	The length of the conical section of the mill [metres].
L_m	The length of the cylindrical section of the mill [metres].

and the net power applied to the charge (P_{charge}) is given by (Apelt *et al.*, 2001)

$$P_{charge} = P_{cylinder} + P_{cone} \quad (2.15)$$

where the equation for the conical section power draw (P_{cone}) is given in equation (2.12) and the cylindrical power draw ($P_{cylinder}$) is given by equation (2.11). For more details on the JKMRC power model refer to Apelt *et al.* (2001) for a detailed summary.

The power draw of the mill can also be calculated by the torque-arm method that has the basic form (Dong and Moys, 2003)

$$P_{torque} = \frac{2\pi}{60} NT \quad (2.16)$$

$$T = F \times d = Mg x_{cog} \quad (2.17)$$

where

P_{torque}	the mill power draw [kW].
N	rotational speed of the mill [RPM].
T	torque [Newton \times metres].
F	force [Newton].
d	torque-arm length [metres].
M	mass of charge in the mill [kg]
g	gravitational acceleration constant [$\frac{\text{meter}}{\text{second}^2}$].
x_{cog}	position of the centre of gravity of the charge [metres].

Dong and Moys (2003) note that the torque-arm power equations assume that the charge shape can be approximated with a cord between the shoulder and toe position, but that this assumption does not hold for a charge at high rotational speeds. Dong and Moys (2003) use position density plots of mills at steady state to obtain the parameters relating to load behaviour, such as the dynamic angle of repose, the shoulder and toe angles to determine



mill power draw from torque-arm power equations more accurately (2.16)-(2.17).

2.3.2.5 Hydrocyclone models

Nageswararao *et al.* (2004) describe two hydrocyclone models that are used in the more popular commercial simulators such as JKSimMet, *Limn* and MODSIM. These packages primarily use cyclone models developed by Nageswararao and Plitt in the 1970s. Newer developments focus on modelling cyclones from fundamental principles through computational fluid dynamics (CFD), but computer power will probably not be sufficient for process simulators for the next 25 years (Nageswararao *et al.*, 2004).

Nageswararao and Plitt both developed empirical models for the hydrocyclone, because the model structure is based solely on experimental data. Nageswararao and Plitt did follow different development methodologies to obtain their models. Nageswararao assumed a structure that explicitly decouples the machine and material characteristics, while Plitt chose an independent variable and equation structure that best fit the available database (Nageswararao *et al.*, 2004).

The models of both Nageswararao and Plitt and a comparison between the models are detailed by Nageswararao *et al.* (2004).

2.3.3 Other models

2.3.3.1 Cumulative breakage rate model

Amestica *et al.* (1993, 1996) developed a mechanistic dynamic model for semiautogenous mills called a *cumulative breakage rate* model. The advantage of this model is that there is only one function describing the breakage kinetics rather than two for selection and breakage function models (Morrell, 2004a). The parameters of the breakage function can be directly and uniquely derived from routine laboratory, pilot and plant data (Hinde, 2007) compared to the parameters of selection and breakage functions that need to be back-calculated (Morrell, 2004a). It still suffers from the same disadvantage as selection and breakage function models that need empirical relationships to relate the parameters of the cumulative breakage function to variations in the milling environment (Hinde, 2007).

2.3.3.2 Transfer function step-test model

The milling control literature favours transfer function models to describe the milling circuit (Chen *et al.*, 2007a, b, 2008, 2009, Craig and MacLeod, 1995, 1996, Pomerleau *et al.*, 2000, Radhakrishnan, 1999, Sbarbaro *et al.*, 2005) that is usually obtained by doing step-tests. Transfer function models obtained through step-tests form part of the more general approach



of linear system identification (Åström and Eykhoff, 1971). The model is obtained by applying step disturbances to the inputs of the plant and measuring the effects on the outputs. The MIMO system is described by a transfer function matrix (for example a three-input, three-output system)

$$G = \begin{bmatrix} g_{11} & g_{12} & g_{13} \\ g_{21} & g_{22} & g_{23} \\ g_{31} & g_{32} & g_{33} \end{bmatrix} \quad (2.18)$$

with each entry describing a specific input-output relationship. The most common form of the transfer function is first order with time delay

$$g_{ij} = \frac{k_{ij}}{\tau_{ij}s + 1} e^{-\theta_{ij}s} \quad (2.19)$$

and integrator with time delay

$$g_{ij} = \frac{k_{ij}}{s} e^{-\theta_{ij}s} \quad (2.20)$$

where k_{ij} is the gain, τ_{ij} is the time constant and θ_{ij} is the time delay associated with the transfer function. The solids feed-rate to mill load and the sump feed water to sump level relationships are usually described by integrators, while the cyclone feed flow-rate to particle size relationship is described by a first order response with time delay.

2.3.3.3 Neural networks

Some authors use neural networks (Bhaumik *et al.*, 1999, Conradie and Aldrich, 2001, Duarte *et al.*, 1999a, 2001) to describe the input-output relationships for use in control systems, which form part of the more general approach of nonlinear system identification (Billings, 1980). Neural networks can learn the complex nonlinear behaviour of a process from its input-output data.

The advantage of using neural networks is that for model-based control, a black box linear or nonlinear model can be constructed very easily from only input-output data.

The disadvantage of using neural networks is that a large amount of data is required to train the neural network properly, but could possibly be offset by allowing online learning at a slow rate (Duarte *et al.*, 1999a). Neural networks that are structured to describe the current output $y(k)$ from the previous plant inputs ($u(k-1), u(k-2), \dots, u(k-N)$) and previous plant outputs ($y(k-1), y(k-2), \dots, y(k-N)$) can be used to study the dynamic of the plant, but it does not extend to neural networks in general, such as neural networks with hidden layers.



Table 2.11: Model internal flows and constants.

Symbol	Description
Volumetric flow-rates used for internal flows: in (<i>i</i>), out (<i>o</i>), underflow (<i>u</i>)	
V_{wi}, V_{wo}, V_{wu}	Water [m^3/hour]
V_{si}, V_{so}, V_{su}	Solids [m^3/hour]
V_{ci}, V_{co}, V_{cu}	Coarse ($V_s - V_f$) [m^3/hour]
V_{fi}, V_{fo}, V_{fu}	Fines [m^3/hour]
V_{ri}, V_{ro}	Rocks [m^3/hour]
V_{bi}, V_{bo}	Balls [m^3/hour]
D_s, D_b	Density of feed ore (D_s) and steel balls (D_b) [kg/m^3]

2.3.4 Mintek mill circuit model modules

Simulation models generate large amounts of data and models usually consist of many states and parameters. This is cumbersome for control and estimation purposes. Mintek developed a research mechanistic model (Coetzee *et al.*, 2009) based on the simulation models (Apelt *et al.*, 2001, Austin *et al.*, 1988, 1983, Morrell, 2004b, Whiten, 1974), but reduced the number of states and parameters to the bare minimum needed for control and estimation purposes.

Mintek gave permission that the following information concerning the model may be published (Coetzee *et al.*, 2009). The model consists of separate modules for the feeder, mill, sump and hydrocyclone. These modules can be connected in various configurations depending on the plant set-up. The model uses five states, namely water, rock, solids, fines and steel balls. Rocks are defined as the ore that is too big to be discharged from the mill. Solids are defined as the coarse ore as well as the fines. Coarse ore is defined as the ore that is discharged from the mill, but is out-of-specification, thus larger than $75 \mu\text{m}$. Fines are defined as the ore that is in-specification and thus smaller than $75 \mu\text{m}$.

The nomenclature for the model is shown in Table 2.11, Table 2.12 and Table 2.13.

2.3.4.1 Feeder module

The feeder module is a very simple one that takes the feed-rate of ore and divides it into the ore streams (fines, coarse and rock) that will be used throughout the model. This module can be replaced by models of real feeders, for example vibratory feeders.



Table 2.12: Model states, inputs and outputs.

Variable	Description
X_{mw}	The holdup of water in the mill. [m ³]
X_{ms}	The holdup of ore in the mill. [m ³]
X_{mf}	The holdup of fine ore in the mill. [m ³]
X_{mr}	The holdup of rock in the mill. [m ³]
X_{mb}	The holdup of balls in the mill. [m ³]
X_{sw}	The holdup of water in the sump. [m ³]
X_{ss}	The holdup of ore in the sump. [m ³]
X_{sf}	The holdup of fine ore in the sump. [m ³]
MIW	The flow-rate of water to the circuit. [m ³ /hour]
MFS	The feed-rate of ore to the circuit (consists of rocks, coarse and fine ore). [tons/hour]
MFB	The feed-rate of steel balls to the circuit. [tons/hour]
α_{speed}	The fraction of critical mill speed.
CFF	The flow-rate of slurry from the sump to the cyclone. [m ³ /hour]
SFW	The flow-rate of extra water to the sump. [m ³ /hour]
PSE	Product particle-size. [% < 75 μ m]
LOAD	The total charge of the mill. [%]
SLEV	The level of the sump. [m ³]
Γ	Rheology factor. [dimensionless]
THROUGHPUT	Product throughput consisting of coarse and fine solids. [tons/hour]
P_{mill}	Power draw of the mill motor. [kW]

The output functions for the feeder unit are given by

$$V_{wo} \triangleq \text{MIW} \quad (2.21)$$

$$V_{so} \triangleq \frac{\text{MFS}}{D_s} (1 - \alpha_r) \quad (2.22)$$

$$V_{fo} \triangleq \alpha_f \cdot \frac{\text{MFS}}{D_s} \quad (2.23)$$

$$V_{ro} \triangleq \alpha_r \cdot \frac{\text{MFS}}{D_s} \quad (2.24)$$

$$V_{bo} \triangleq \frac{\text{MFB}}{D_b} \quad (2.25)$$

2.3.4.2 Mill module

The mill module is capable of modelling various mill types such as rod, ball, SAG and AG mills. It is similar to the models found in literature, but adds the effect of mill power and slurry rheology (Shi and Napier-Munn, 2002) to the breakage and power functions.

It receives the ore, balls and water and incorporates models that describe the production of fines, rock consumption, ball wear, outflow for various discharge mechanisms e.g. grate discharge, power consumption and rheology effects.

The rheology factor which relates to the fluidity of the slurry in the mill (Bazin and B-



Table 2.13: Model Parameters.

Parm	Description
α_f	Fraction of fines in the ore. [dimensionless]
α_r	Fraction of rock in the ore. [dimensionless]
ϕ_f	Power per fines produced. [kW·hr/ton]
ϕ_r	Rock abrasion factor. [kW·hr/ton]
ϕ_b	Steel abrasion factor. [kW·hr/ton]
P_{\max}	Maximum mill motor power. [kW]
v_{mill}	Mill volume. [m ³]
$v_{P_{\max}}$	Mill filling volume for maximum power. [m ³]
$\Gamma_{P_{\max}}$	Rheology factor for maximum mill power. [dimensionless]
ε_{ws}	Maximum water-to-solids volumetric ratio at zero pulp flow. [dimensionless]
V_V	Volumetric flow per “flowing volume” driving force. [hr ⁻¹]
δ_{Pv}	Power-change parameter for volume. [dimensionless]
δ_{Ps}	Power-change parameter for fraction solids. [dimensionless]
α_P	Fractional power reduction per fractional reduction from maximum mill speed. [dimensionless]
α_{ϕ_f}	Fractional change in kW/fines produced per change in fractional filling of mill. [dimensionless]
χ_P	Cross-term for maximum power. [dimensionless]
ε_c	Cyclone coarse split fraction. [dimensionless]
α_{su}	Fraction of solids in the underflow of the cyclone. [dimensionless]
C_1	Constant. [dimensionless]
C_2	Constant. [dimensionless]
C_3	Constant. [dimensionless]
C_4	Constant [dimensionless]



Chapleau, 2005, Shi and Napier-Munn, 1996, 2002) is calculated as

$$\Gamma \triangleq \left\{ \frac{\max \left[0, \left(X_{mw} - \left(\left(\frac{1}{\varepsilon_{ws}} \right) - 1 \right) X_{ms} \right) \right]}{X_{mw}} \right\}^{0.5} \quad (2.26)$$

and the mill power as

$$P_{\text{mill}} \triangleq P_{\text{max}} \cdot \left\{ 1 - \delta_{Pv} Z_v^2 - 2 \cdot \chi_P \cdot \delta_{Pv} \cdot \delta_{Ps} \cdot Z_v \cdot Z_\Gamma - \delta_{Ps} \cdot Z_\Gamma^2 \right\} \cdot (\alpha_{\text{speed}})^{\alpha_P} \quad (2.27)$$

where load is represented by

$$Z_v \triangleq \frac{X_{mb} + X_{mr} + X_{ms} + X_{mw}}{v_{P_{\text{max}}} \cdot v_{\text{mill}} - 1} \quad (2.28)$$

and rheology is represented by

$$Z_\Gamma \triangleq \frac{\Gamma}{\Gamma_{P_{\text{max}}}} - 1. \quad (2.29)$$

The production of fines is a linear function of the total mill volume filling (LOAD $\triangleq (X_{mw} + X_{ms} + X_{mr} + X_{mb})$).

$$\text{FP} \triangleq \frac{P_{\text{mill}}}{D_s \cdot \left\{ \phi_f \cdot \left[1 + \alpha_{\phi_f} \cdot \left(\frac{\text{LOAD}}{v_{\text{mill}}} - v_{P_{\text{max}}} \right) \right] \right\}} \quad (2.30)$$

The fines produced from rocks are not distinguished from fines produced from the coarse ore.

The rocks in the mill grind down to coarse and/or fines in indeterminable ratios. The total fines produced are modelled to come from both rocks and coarse material. The yield of coarse and fines from rocks will therefore not be modelled, only the consumption of rocks. The consumption is at it highest with high power, fluid slurry and relatively low amounts of fine and coarse ore. The model for rock consumption is given by

$$\text{RC} \triangleq \left(\frac{1}{D_s \cdot \phi_r} \right) \cdot P_{\text{mill}} \cdot \Gamma \left(\frac{X_{mr}}{X_{mr} + X_{ms}} \right) \quad (2.31)$$

The steel balls in the mill grind away over time. The consumption of the steel balls is at its highest with high power, fluid slurry and high ball loadings and the consumption can be described as

$$\text{BC} \triangleq \left(\frac{1}{D_b \cdot \phi_b} \right) \cdot P_{\text{mill}} \cdot \Gamma \cdot \left(\frac{X_{mb}}{X_{mb} + X_{mr} + X_{ms}} \right) \quad (2.32)$$



The volumetric flows from the mill are described by

$$V_{to} \triangleq V_V \cdot \Gamma \cdot X_{mw} \quad (2.33)$$

$$V_{wo} \triangleq V_{to} \cdot \left(\frac{X_{mw}}{X_{ms} + X_{mw}} \right) \quad (2.34)$$

$$V_{so} \triangleq V_{to} \cdot \left(\frac{X_{ms}}{X_{ms} + X_{mw}} \right) \quad (2.35)$$

$$V_{fo} \triangleq V_{to} \cdot \left(\frac{X_{mf}}{X_{mr} + X_{mw}} \right) \quad (2.36)$$

where $V_{bo} \triangleq 0$ and $V_{ro} \triangleq 0$ because it is assumed that the rocks and balls cannot escape through the discharge grate.

The changes in volumetric holdups in the mill are described as

$$\frac{dX_{mw}}{dt} \triangleq V_{wi} - V_{wo} \quad (2.37)$$

$$\frac{\partial X_{ms}}{\partial t} \triangleq V_{si} - V_{so} + RC \quad (2.38)$$

$$\frac{\partial X_{mf}}{\partial t} \triangleq V_{fi} - V_{fo} + FP \quad (2.39)$$

$$\frac{\partial X_{mr}}{\partial t} \triangleq V_{ri} - RC \quad (2.40)$$

$$\frac{\partial X_{mb}}{\partial t} \triangleq V_{bi} - BC \quad (2.41)$$

2.3.4.3 Mixed-sump module

The mixed-sump module assumes that the water, fines and coarse material are fully mixed. The sump only handles water, fine and coarse ore because it is assumed that the rock and the balls remain in the mill.

The volumetric flow-rates from the sump are described as

$$V_{wo} \triangleq CFF \cdot \left(\frac{X_{sw}}{X_{ss} + X_{sw}} \right) \quad (2.42)$$

$$V_{so} \triangleq CFF \cdot \left(\frac{X_{ss}}{X_{ss} + X_{sw}} \right) \quad (2.43)$$

$$V_{fo} \triangleq CFF \cdot \left(\frac{X_{sf}}{X_{ss} + X_{sw}} \right) \quad (2.44)$$



The changes in hold-ups in the sump are described by

$$\frac{\partial X_{sw}}{\partial t} \triangleq V_{wi} + \text{SFW} - V_{wo} \quad (2.45)$$

$$\frac{\partial X_{ss}}{\partial t} \triangleq V_{si} - V_{so} \quad (2.46)$$

$$\frac{\partial X_{sf}}{\partial t} \triangleq V_{fi} - V_{fo} \quad (2.47)$$

The sump level is defined as

$$\text{SLEV} \triangleq X_{sw} + X_{ss}. \quad (2.48)$$

The cyclone feed density is defined as

$$\text{CFD} \triangleq X_{sw} + D_s \cdot X_{ss} / X_{sw} + X_{ss} \quad (2.49)$$

2.3.4.4 Hydrocyclone module

The hydrocyclone is a classification device that splits a slurry feed with regard to weight, which usually relates to the size of the particles. Lighter particles are forced out at the overflow of the cyclone, while the heavier particles are forced out at the underflow. The cyclone model is designed to model the product size and density accurately by taking the effects of angular velocity of the particle inside the cyclone, slurry density and viscosity into account. The model is based on the empirical hydrocyclone models of Plitt and Nageswararao (Nageswararao *et al.*, 2004). The flow-rates of the various constituents of the slurry at the underflow of the hydrocyclone are defined as

$$V_{cu} \triangleq V_{ci} \cdot \left(1 - C_1 \cdot e^{\left(-\frac{V_{ii}}{\varepsilon_c}\right)}\right) \times \left(1 - \left(\frac{F_1}{C_2}\right)^{C_3}\right) \cdot \left(1 - P_i^{C_4}\right) \quad (2.50)$$

$$F_u \triangleq 0.6 - (0.6 - F_i) \cdot e^{\left(-\frac{V_{cu}}{\alpha_{su}\varepsilon_c}\right)} \quad (2.51)$$

$$V_{wu} \triangleq V_{wi} \cdot \frac{(V_{cu} - F_u \cdot V_{cu})}{(F_u \cdot V_{wi} + F_u \cdot V_{fi} - V_{fi})} \quad (2.52)$$

$$V_{fu} \triangleq V_{fi} \cdot \frac{(V_{cu} - F_u \cdot V_{cu})}{(F_u \cdot V_{wi} + F_u \cdot V_{fi} - V_{fi})} \quad (2.53)$$

$$F_i \triangleq \frac{V_{si}}{V_{wi} + V_{si}} \quad (2.54)$$

$$P_i \triangleq \frac{V_{fi}}{V_{si}} \quad (2.55)$$

The product particle size is defined as

$$\text{PSE} \triangleq \frac{V_{fo}}{(V_{co} + V_{fo})} \quad (2.56)$$



where $V_{fo} \triangleq V_{fi} - V_{fu}$ and $V_{co} \triangleq V_{ci} - V_{cu}$. The product throughput is defined as

$$\text{THROUGHPUT} \triangleq V_{co} + V_{fo}. \quad (2.57)$$

2.4 CONCLUSION

This chapter gives an overview of the milling process and the different simulation models available for modelling milling circuits. The more complex models are usually employed to simulate the milling circuit and generate vast amounts of data for circuit design and analysis. The simpler models are usually employed in controllers and controller design.

This chapter outlines the nonlinear model developed by Mintek (Section 2.3.4) that consists of models for the mill, cyclone and sump and will be used in later chapters as the prediction model for the milling circuit as well as the simulation model. The Mintek model is modular to simulate different milling circuit configurations easily.